

Cryogenic Neuromorphic Hardware

Md Mazharul Islam¹, Shamiul Alam¹, Md Shafayat Hossain², Kaushik Roy³ and Ahmedullah Aziz^{1*}

¹Dept. of Electrical Eng. & Computer Sci., University of Tennessee, Knoxville, TN, 37996, USA

²Dept. of Physics, Princeton University, Princeton, NJ, 08544, USA

³Dept. of Electrical and Computer Engineering, Purdue University, West Lafayette, IN, 47906, USA

*Corresponding Author's Email: aziz@utk.edu

Abstract- The revolution in artificial intelligence (AI) brings up an enormous storage and data processing requirement. Large power consumption and hardware overhead have become the main challenges for building next-generation AI hardware. Therefore, it is imperative to look for a new architecture capable of circumventing these bottlenecks of conventional von Neumann architecture. Since the human brain is the most compact and energy-efficient intelligent device known, it was intuitive to attempt to build an architecture that could mimic our brain, and so the chase for neuromorphic computing began. While relentless research has been underway for years to minimize the power consumption in neuromorphic hardware, we are still a long way off from reaching the energy efficiency of the human brain. Besides, design complexity, process variation, etc. hinder the large-scale implementation of current neuromorphic platforms. Recently, the concept of implementing neuromorphic computing systems in cryogenic temperature has garnered immense attention. Several cryogenic devices can be engineered to work as neuromorphic primitives with ultra-low demand for power. Cryogenic electronics has therefore become a promising exploratory platform for an energy-efficient and bio-realistic neuromorphic system. Here we provide a comprehensive overview of the reported cryogenic neuromorphic hardware. We carefully classify the existing cryogenic neuromorphic hardware into different categories and draw a comparative analysis based on several performance metrics. Finally, we explore the future research prospects to circumvent the challenges associated with the current technologies.

Keywords: Cryogenic, Josephson junction, neuromorphic, quantum phase slip junction, superconducting nanowire.

I. Introduction

With the advent of artificial intelligence as one of the leading decision-making pathways in modern technology, it is getting harder to process and store an enormous amount of data in conventional von Neumann architecture [1], [2]. Moreover, the evolution of microelectronic circuits for almost half a century has reached a fundamental bottleneck where miniaturization of electronic devices has become challenging due to several practical concerns [3]. The massive expansion of data has the drawback of excessive power consumption. For example, the US data centers consume terawatt-hour (TWh) range of power nowadays [4]. Furthermore, several device reliability issues emerge as a major concern for short-channel

devices. These unassailable challenges have led us to look for a fundamentally new architecture for computation and storage devices. From neuroscience, we know that the human brain can process an enormous amount of data only by consuming around 20 W [5] of power. Our brain can perform complex tasks operating at an ultra-low frequency (few Hertz), thanks to the high degree of parallelism in its architecture [6]. So, it is intuitive to try to mimic the biological brain to build a novel architecture and on this basis, neuromorphic computing has emerged [7]. In our brain, information is transmitted in the form of spike between neurons and synapses [8], [9]. By mimicking this behavior, spiking neural network (SNN) has emerged as the next-generation neural network which imitates the biological spiking behavior as the primary information processing scheme [10]–[12].

Although the existing software implementations of spiking neural network are precise and flexible, they are expensive in terms of computation and power efficiency [13]–[15]. Thus, researchers have been trying to build a dedicated hardware platform for SNN-based algorithm processing. Several device platforms based on memristor, magnetic materials, phase change materials (PCM), and complementary metal-oxide-semiconductor (CMOS) have been explored and implemented. Spiking neural network implementation based on these devices relies on the intrinsic dynamics of the device to emulate biological realism [16], [17], [26], [18]–[25]. But they are still far behind the human brain in terms of power efficiency. Also, process variation has become a major concern for large-scale architecture implementation [27]. For this reason, researchers are constantly exploring novel platforms with higher energy efficiency and scalability.

The primary source of power consumption in a large neuromorphic network is the massive interconnectivity between the neurons and synapses [28]. In this context, superconducting devices have lossless characteristics which incite them to be incorporated in low power interconnectivity in a neuromorphic network [29]. Besides, superconducting devices manifest switching characteristics with unprecedented power consumption and ultra-high-speed. Also, several non-superconducting materials such as NbO_x exhibit neuromorphic characteristics in cryogenic temperature [30]. The extraordinary power consumption of these designs evidently indicates that neuromorphic hardware based on cryogenic devices can open a new era of next-generation ultra-low power and compact neuromorphic hardware.

In this review, we discuss state-of-the-art cryogenic neuromorphic hardware. We organize our discussions as the following: in section II, we discuss the motivation for exploring

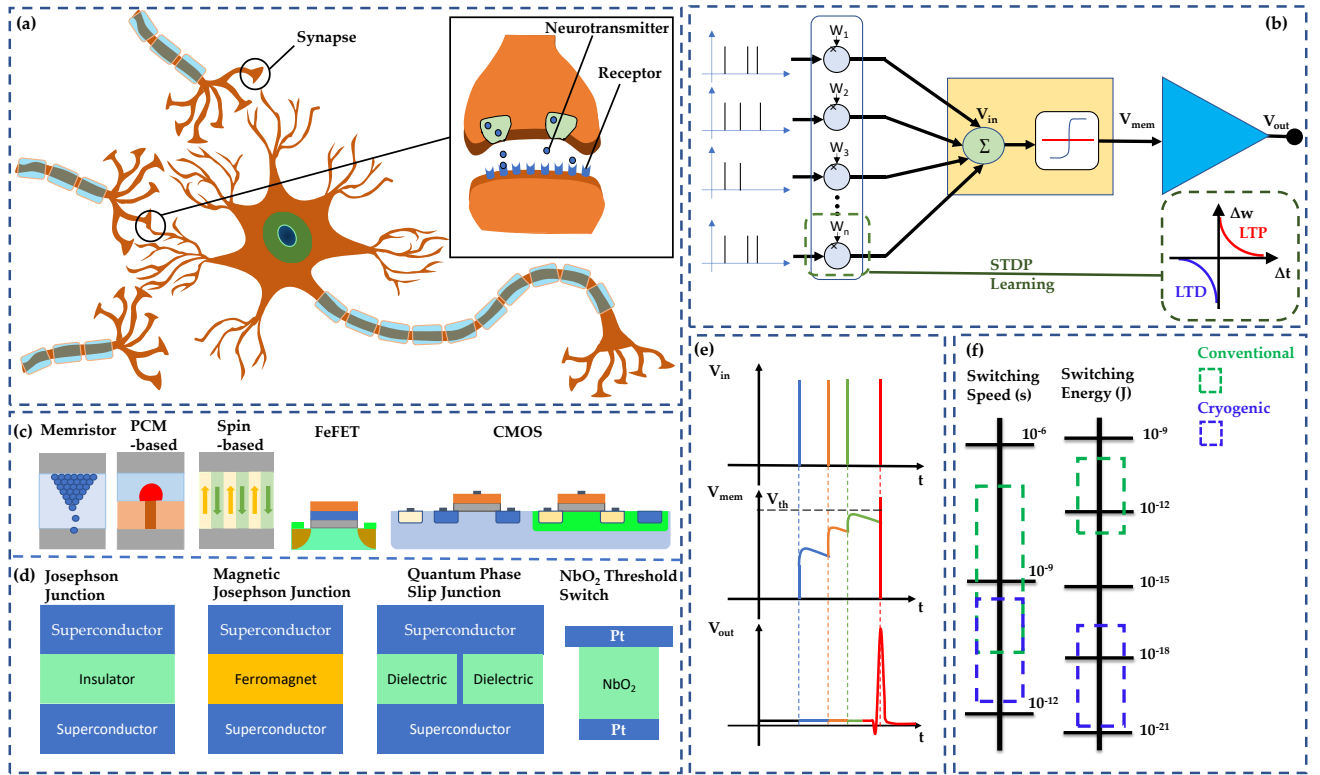


Figure 1: (a) Biological neuron connected with multiple neurons through synapses, inset shows the transportation of neurotransmitter. (b) Electronic model of a neuromorphic system, the three mentioned voltage values (V_{in} , V_{mem} , and V_{out}) are depicted in (e). (c) Conventional neuromorphic hardware. (d) Cryogenic platforms for neuromorphic hardware. (e) Input spikes (V_{in}), corresponding membrane potential (V_{mem}) and output spike (V_{out}) of a leaky integrating and fire neuron after V_{mem} crosses the threshold voltage (V_{th}). (f) Rough comparison of switching speed and energy comparison of conventional and cryogenic hardware.

cryogenic neuromorphic hardware and the primary advantages of these architectures. In section III, we shed the light on different cryogenic neuromorphic hardware where both superconducting and non-superconducting designs are analyzed. In section IV, we present a comparative analysis among different methodologies and discuss the major challenges faced by different cryogenic neuromorphic platforms. Finally, we conclude our discussion with several research prospects.

II. Why Cryogenic Neuromorphics?

For an efficient neuromorphic network, the network system should have sufficient power efficiency, bio-realism, and compactness compared to the human brain. Our brain has several distinct features that make it different from a computer. In the core of our brain's building block, neurons, synapses, axons, dendrites are the most significant components [see Fig. 1(a) and Fig. 1(b) for the biological and electronic representation of a neuromorphic system, respectively]. Neurons are spiking element which generates spikes and synapses control the signal transport between neurons through adjustable connectivity strength. Fig. 1(e) illustrates the behavior of a spiking neuron. There are 86 billion neurons in the human brain and each one is connected to thousands of others through synapses [31]. This massive interconnectivity enables our brain to be compact (around 1.5 kg in weight and 1260 cm³ in volume) and highly energy-efficient (20 W of power consumption) [32]–[34]. Thus, the neuromorphic platform should be less dissipative so that a high degree of

parallelism can be achieved. There are several challenges associated with the conventional platforms which limits their performance in practical implementation.

- (i) It is a major challenge to incorporate them in a large network with dissipative interconnections [35], where the resistive loss becomes significant and results in inefficiency.
- (ii) Bio-realism is a crucial requirement for a network to be brain-like [36]–[38]. Inherent characteristics of a device determine the degree of bio-realism that can be achieved through the design approach[39]. Although conventional neuromorphic hardware exhibits a varying degree of bio-realism, most of them lack design simplicity. Simpler design implies fewer devices for each unit cell of neurons or learning circuits which implies less area.
- (iii) Another bottleneck of conventional hardware platform is their operating frequency. For high-frequency operations, the switching time should be fast [40]. Most of the conventional platforms are limited in terms of operating frequency [28].
- (iv) There are other individual drawbacks associated with each of the technologies. Although CMOS devices can operate at very low temperatures (4K), CMOS-based neuromorphic devices are still disadvantageous due to several reliability issues [41]–[43]. For example, due to hot-carrier effects, the device lifetime decreases significantly [44]. Moreover, it is challenging to design CMOS circuits with biological realism due to massive design complexity. Resistive switching-based devices such as memristor and MTJ based neuromorphic devices are

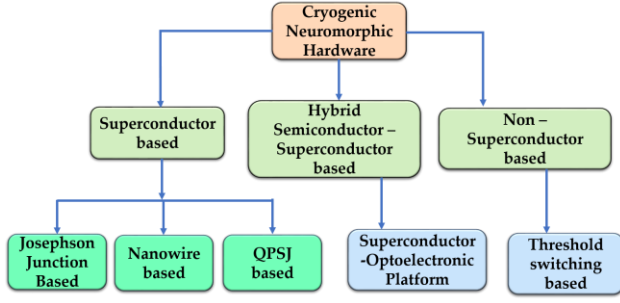


Figure 2: Hierarchy of the classification of state-of-the-art cryogenic neuromorphic hardware.

being widely explored for their high scalability [10],[45]. But at low temperatures, resistance variation occurs due to the geometric fluctuations of the filament in the memristor [46]. Also, memristors suffer from low endurance, high latency, and are prone to device variation whereas MTJ suffer from a low ON/OFF ratio and low density [16], [47], [48].

Because of these challenges, it is difficult to build an efficient neuromorphic network in conventional platforms that is integrable on a large scale. Therefore, a novel platform that can resolve these challenges can pave the way to next generation neuromorphic network with ultra-low power consumption and immense integrability.

Superconducting materials and devices are well known for their lossless characteristics and therefore it is an obvious choice of exploration to design ultra-low power neuromorphic circuits. Josephson junction (JJ), quantum phase slip junction

(QPSJ), and superconducting nanowire switch states with minuscule power which is completely unprecedented in the conventional hardware platforms [49]–[51]. Ultrafast switching behavior in these devices enables them to operate even in hundreds of GHz of frequency which enables them to operate in a larger range of frequency than the conventional platforms [50], [52]. Apart from the superconducting devices, non-superconducting devices such as NbO_x also exhibit a fast switching characteristics in low temperatures for which they have been reported in the cryogenic neuromorphic circuit operating in the GHz range of frequency [53]. Also, the inherent characteristics of these devices are suitable for bio-realistic neuromorphic behavior in a much simpler design. Fig. 1(f) shows the comparison of speed and energy between the conventional and cryogenic neuromorphic platforms.

Moreover, the operating temperature of these devices brings the added advantage of them being used in cryogenic applications. For example, the peripheral control of quantum computers can highly benefit from a cryogenic neuromorphic platform [54]. The parameter of a quantum circuit can be trained by neuromorphic hardware. D. Marković *et al.* have demonstrated a neural network that has been implemented in brain-inspired quantum hardware to accelerate the computation process [54]. Also, a cryogenic environment offers much higher noise immunity comparative to non-cryogenic circuits and systems [55]. This is a significant advantage since noise can affect the overall performance to the electrical oscillator used in a neuromorphic system [26], [56]. The performance of analog neuron is also affected by several internal and external noise sources. Finally, cryogenic devices have excellent thermal properties required for aerospace applications [57].

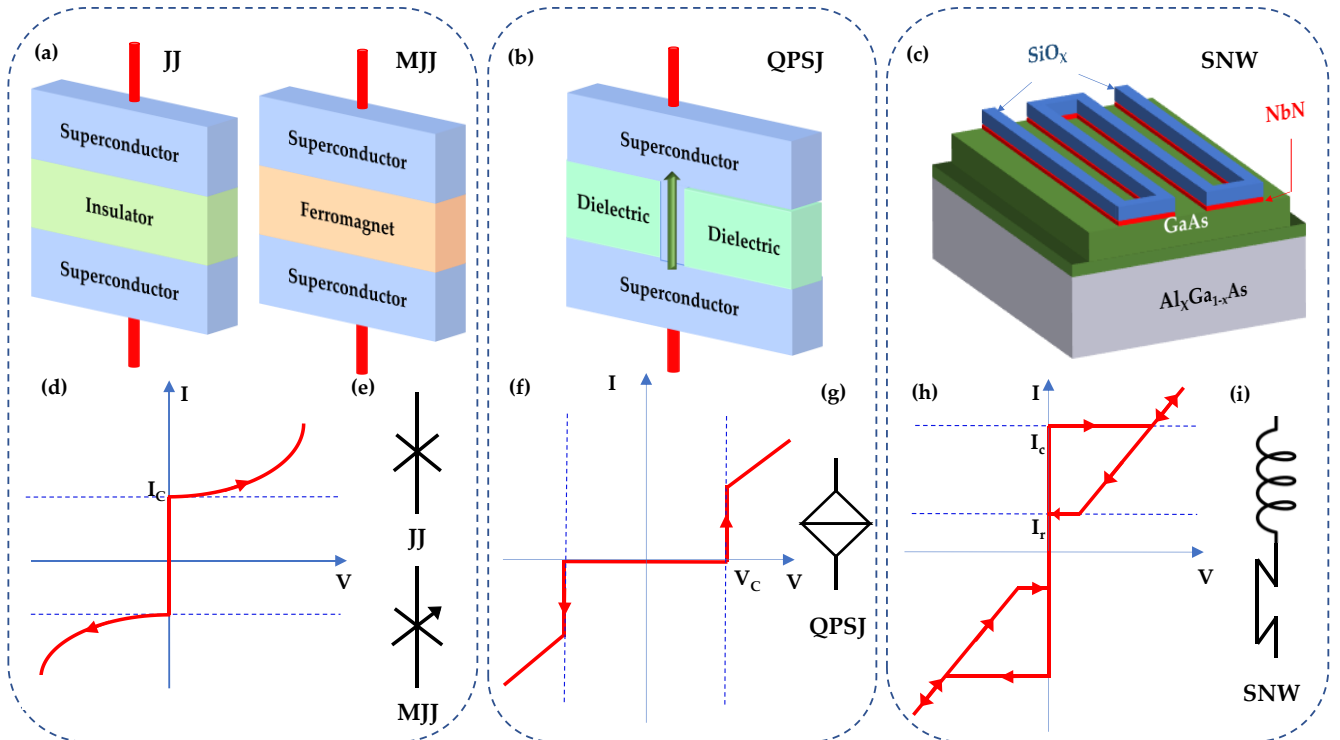


Figure 3: Structure of (a) an SIS Josephson junction and magnetic Josephson junction, (b) a quantum phase slip junction, and (c) a superconducting nanowire. (d) I-V characteristics and (e) symbol of Josephson Junction (JJ) and Magnetic Josephson junction (MJJ). (f) I-V characteristics and (g) symbol of quantum phase slip junction (QPSJ). (h) I-V characteristics and (i) symbol of superconducting nanowire (SNW).

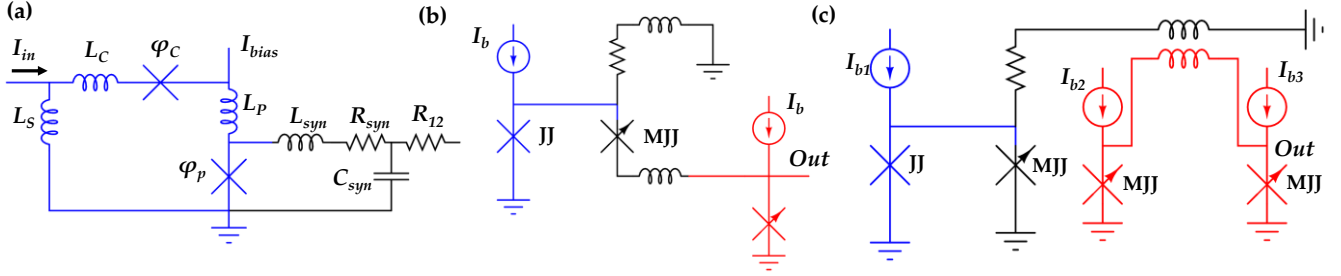


Figure 4: Three different circuit topologies of Josephson junction-based neuromorphic circuit [39] [62] [63]. Blue, black, and red colors signify pre-synaptic neuron, synapse, and post-synaptic neuron.

III. State-of-the-art Cryogenic Neuromorphic devices

So far, several cryogenic hardwares have been proposed as potential neurons and synapses in a neuromorphic network. We primarily classify the state-of-the-art cryogenic neuromorphic hardware based on the core cryogenic device. The classification scheme is outlined in Fig. 2.

III.A. Superconductor-based Neuromorphic Hardware

We start with superconducting device-based neuromorphic designs. Several superconducting devices such as JJ, QPSJ, superconducting nanowire have been utilized to design energy-efficient neuromorphic circuits. Figure 3 demonstrates the physical structure of these devices and their typical I - V characteristics which manifest abrupt switching, suitable for the generation of spikes. As important as the spiking and plasticity characteristics, a neuromorphic architecture must have the ability to transport spikes over long distances without any significant power dissipation. In a superconductor transmission line, the loss is minimal, and the dispersion is also low up to a certain frequency. This frequency is known as gap frequency, $f_g (= 2\Delta_{sc}/h)$ [58]. In most of the superconducting circuits, Nb transmission line is used for which the gap frequency is reported as much as 650 GHz. A single flux quantum (SFQ) pulse with a duration of 1 ps can travel up to 10 mm distance without significant loss and dispersion [58][59]. If the inherent power consumption is considered, then superconducting circuits consume considerably less energy. We discuss several superconductor-based neuromorphic hardware in the subsequent discussion.

III.A.1. JJ-based Neurons and Synapses

In a JJ, two superconducting regions are separated by an insulating region through which cooper pair tunneling occurs [60]. Ballistic transport of digital signal can be passed through this tunneling junction with ultra-high speed ($\sim 1/100^{\text{th}}$ of the speed of light) [61]. Above a sufficiently high current, (I_c), the junction becomes resistive, and voltage drop begins to appear across the junction. The switching from superconducting to resistive state occurs in ps timescale. The ultra-fast switching speed (~ 1.5 ps) of JJ and simple architecture makes it suitable for various types of design consideration. When the phase difference of the two superconducting regions whirls over once, a magnetic pulse is produced which is known as SFQ [64]. The flux has the same shape and duration each time it is being produced. Using these virtues of JJ, several neurons and synapses have been proposed.

Crotty *et al.* [39] proposed a current biased JJ-based spiking neuron in 2010 [Fig. 4(a)]. Here, two JJs combinedly work to produce neuronal spiking. These JJs are referred to as control junction and pulse junction. The neuron loop is connected to another Resistor (R) - Inductor (L) - Capacitor (C) loop that mimics electrical and chemical synapse [Fig. 4(a)]. When a bias current (I_{bias}) is applied, it is divided to both the JJs. I_{bias} keeps both the JJs just below critical current. If an input current (I_{in}) with sufficient amplitude is applied, the current through the pulse junction exceeds its I_c , which injects a magnetic flux into the loop. This magnetic pulse creates a voltage drop across the pulse junction which creates the action potential (AP). As the flux builds, the current through the control junction reaches a critical value which eventually drains the flux in the loop. This

Table I: Structural comparison of existing JJ-based neuromorphic hardware.

Design	Input Neuron	Output Neuron	Synaptic Element	Synapse Type
Crotty <i>et al.</i> [39]	Current biased JJ loop	-	RC resonant circuit	Binary
Schneider <i>et al.</i> [62]	Current biased JJ	Current biased MJJ	Dynamically reconfigurable MJJ	Graded Weight
Schneider <i>et al.</i> [63]	Current biased JJ	Current biased SQUID	Dynamically reconfigurable MJJ	Graded Weight
Schneider <i>et al.</i> [58]	-	SQUID with resistive element	MJJ	Graded Weight
Goteti <i>et al.</i> [64]	Multiple JJ structure	-	SQUID loop	Graded Weight

way the pulse junction retains its initial superconducting state and gets prepared to fire again in the next cycle. The firing rate of this design is reported to be 2.0×10^{10} AP/(neuron/s). It is theoretically shown that two individual neurons can be coupled together to implement both excitatory and inhibitory synaptic coupling depending on the sign of the bias current. For positive (negative) bias current, the second loop works as an excitatory (inhibitory) synapse. The inherent energy consumption of the circuit (without considering the cooling power) has been measured by the SFQ pulse of each of the JJs which is 70 zJ, 35 zJ, and 150 zJ for the input neuron, synapse MJJ, and output JJ.

Although Crotty *et al.* [39] demonstrated excitatory and inhibitory synaptic behavior, their design does not contain the implementation multistate synaptic weight and the dynamic tunability in the synaptic weight. Schneider *et al.* built a neuromorphic element where both non-magnetic and magnetic JJs were utilized and the critical current of the magnetic Josephson junction (MJJ) is dynamically tunable [62]. Here, only a current biased JJ is used as a neuron element. The MJJ is kept in the middle of two neurons, which weights the transmitted pulse from the input neuron to the output neuron [Fig. 4(b)]. The preneuron JJ produces spikes which is weighted in the MJJ. The critical current of this MJJ (from 1 μ A to 100 μ A) is analogous to the synaptic weight in a neuromorphic network and can be dynamically tuned by changing the superconducting order parameter. The output neuron has a higher critical current (100 μ A to 500 μ A) and can fire based on the critical current of synaptic MJJ. This design reports a firing frequency of 0.35 GHz. The total energy for a single classification is roughly 2 aJ (= 2 fJ with refrigeration) which is comparable to the energy required for a single human synaptic event (10 fJ). Although, the proposed circuit exhibits neurosynaptic behavior in simulation, critical current modulation practically can be disadvantageous for crosstalk between MJJ synapses.

In a subsequent work, Schneider *et al.* utilized a nanotextured MJJ as a synapse where a zero-field (0 T) reproducible analog control is demonstrated for the first time [63]. Here, they used a Si layer containing Mn nanoclusters as the tunneling barrier. The magnetic order of the Mn nanoclusters was tuned to vary the critical current of the MJJ. The critical current of the disordered state is higher than the critical current in the ordered state. To increase the synaptic weight (decrease the magnetic order of the nanocluster) electrical current pulses (4 pJ and 1 ns duration) at zero applied magnetic field need to be applied. To decrease the synaptic weight (increase magnetic order), current pulses were applied in the presence of an external magnetic field (~ 5 T). The number of electrical pulses and the pulse energy can finetune the critical current. The energy for a JJ synapse with an elliptical cross-sectional area of $1.5 \times 3.5 \mu\text{m}^2$ is 3 aJ [63]. Contrary to the previous work, here the post neuron is inductively coupled to the synaptic branch with a 50% coupling strength and this coupling works as dc to SFQ converter. This inductively coupled structure reduces unwanted crosstalk between different circuit structures. Here, the estimated energy for a presynaptic spike weighted to generate a post-synaptic spike was reported as ~ 1 aJ. For a large-scale system ($N \sim 1000$), the energy would be ~ 1 fJ with the additional cost of cooling. Besides, SFQ based circuits have been previously reported to work up to 60

gigabits/s from which it can be estimated to operate in hundreds of GHz range of frequency.

In their following work, Schneider *et al.* proposed the concept of coupling between multiple synapses with output neurons in a large-scale network [58]. Here all the synapses are connected to a large output neuron by inductive coupling and the signals in the synapses are integrated in the neuron loop. The current through the JJ in the large neuron loop exceeds the critical value or not based on the inputs of the synaptic circuits, and if it does, an SFQ pulse is created. The critical current of the synapse MJJs are modulated in supervised fashion. This inductively coupled connection is designed to minimize unwanted cross-talks between inductively coupled circuit structures. In another work, the relationship of the inductively coupled current with output SQUID neuron is analyzed and it is found that the coupled current level increases up to a certain value with the increase of the pulse duration but saturates after that point [64]. Goteti *et al.* has proposed a neural network with a disordered JJ array synaptic network where JJ based collective disordered synaptic network works with neuron element to implement feedback loops for unsupervised learning algorithm [65]. Here, a disordered array of n -different loops can have a $3n$ memory state.

To implement parallelism in a network, sufficient fan-in and fan-out capacity are required in a technology platform. Schneider *et al.* has reported a theoretical demonstration of a fanout of 1-to-10000 and a fan-in of 100-to-1 [66]. A rough estimate of the power dissipated for a 1-to-128 flux-based fan-out circuit for a given critical current value is reported to be 44 aJ. Both current-based and flux-based fan-in is analyzed, and it is demonstrated that for larger network signal current reduces significantly for current-based fan-in circuits. Therefore, for larger network flux-based fan-in is more efficient. The minimum diameter of a typical JJ is 500 nm [66] whereas MJJs for neuromorphic application has a cross-sectional area of a few μm^2 ; this is several orders of magnitude larger than conventional CMOS-based designs [67]. However, for cryogenic memory applications, MJJs with cross-sections as low as $50 \text{ nm} \times 100 \text{ nm}$ has been reported. Hence, cryogenic neuromorphic hardware based on MJJ is expected to reach similar size. Although, miniaturization of MJJ size is an encouraging factor for digital implementation of MJJ synapse. for an analog MJJ-based synapse, reducing the size will reduce the number of nanoclusters and thus the number of synaptic states available. Based on these design aspects, it is evident that JJ-based neuromorphic circuits show promising performance in their neuro-synaptic behavior in terms of speed and power efficiency. Since, a full-scale neuromorphic network based on JJ requires constant current biases with active interconnects, further research is still necessary for a fully JJ-based efficient and scalable neuromorphic network.

III.A.2. QPSJ-based neuromorphic hardware

Even though JJ-based designs reported so far exhibit neurosynaptic behavior with ultra-low power consumption, their designs include constant current biasing which is not suitable for a voltage-based operation. QPSJ is an alternative

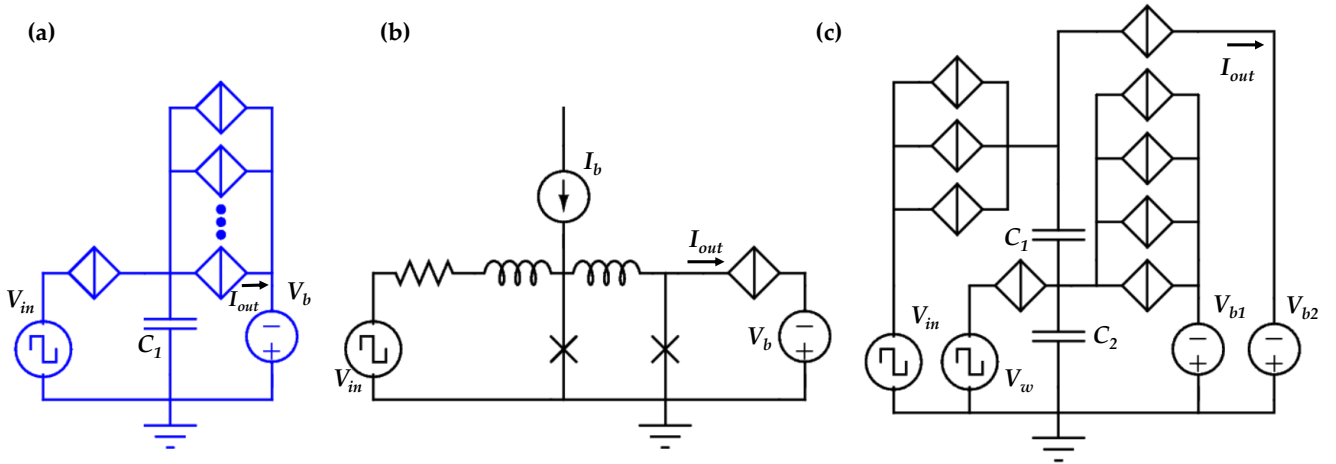


Figure 5: (a) QPSJ based neuron [72]. (b) Multistate synaptic circuit based on current biased JJ and QPSJ [76]. (c) Multistate synaptic circuit based on QPSJ [73].

superconducting device that comes into consideration for its voltage-based switching approach. Quantum phase slip can be characterized as the dual process to the Josephson effect based on the charge-flux duality. In a QPSJ, flux-quantum tunnels across a superconducting nanowire along with the cooper pair transport and generates a voltage across the junction [68]. Mooji *et al.* has reported a QPSJ with Nb-Si wire which has 3 μm length [69]. Phase slip event can be expected in superconducting wires with diameter as low as 10 nm [70]. The nm range of thickness indicates that it QPSJ can be incorporated in compact neuromorphic network. In a QPSJ, below a certain threshold voltage (critical), no current flows due to Coulomb blockade [71]. When an input voltage is above the threshold value, the cooper pair begins to tunnel through the junction and the current begins to flow. Therefore, the I - V curve of a QPSJ is analogous to the V - I curve of a JJ. When a voltage pulse is applied across a QPSJ, it generates a spike naturally.

By utilizing this switching behavior of QPSJ, Cheng *et al.* have proposed a QPSJ-based spiking neuron for the first time in 2018 [72]. In their design, two QPSJs are connected through a capacitor in between, which acts as an island of charge between them. Here, the first QPSJ is connected to the input. For an incoming input, voltage across it rises. When the capacitance is smaller than a certain value ($C_1 < 2e/V_C$, V_C being the critical voltage of the junction), the neuron produces spike output for every spike input. This mode of operation is known as the tonic spiking mode. If the capacitance is above this value, the neuron works in tonic bursting mode. In this case, the input voltage pulses are integrated and the output current spikes are fired once a certain threshold is reached. This design enables tunable firing frequency and threshold voltage. The second QPSJ is kept at a bias voltage V_b . The firing frequency can be varied by changing the series resistance of the QPSJ devices used. Besides, threshold voltage and firing rate both can be tuned by connecting several QPSJs in parallel [Fig. 5(a)]. To keep all the QPSJs equally biased, a resistor can be inserted, and the behavior perfectly matches with a LIF neuron behavior. The total firing energy for this circuit design is found by the switching energy of QPSJ multiplied by the number of QPSJ required for firing. In the parallel branch, for only one QPSJ, the energy is 6.4 zJ ($3.2 \text{ zJ} \times 2$). This work reported only the

spiking behavior of the neuron and kept the design of a synaptic circuit for further exploration.

QPSJ has also been reported in novel neurosynaptic circuit in combination with JJ [Fig. 5(b)]. In the subsequent work, Cheng *et al.* have combined the previously proposed QPSJ neuron with a synaptic circuit based on MJJ [72]. The tunable critical current of the MJJ works as the synaptic weight for the device. When, the current across the first JJ reaches the critical value, current is bypassed to the second JJ and a voltage appears across it. This eventually increases the voltage across the QPSJ and switches it to the initial superconducting state. Both a binary and multistate synaptic circuit has been proposed. In the binary synapse, an input voltage pulse can generate an output current spike based on the critical current of MJJ. Four-state synaptic behavior has been demonstrated by using two MJJs in parallel instead of using one, where four different levels of the critical current of the biased MJJ determines four synaptic states. Here, the synaptic weight (critical current) will determine the number of output spikes in a given period (2, 1, 0.5, 0). By increasing the number of JJs, the number of synaptic states can be increased.

A complete neuromorphic network solely based on QPSJ has been firstly demonstrated by Cheng *et al.* [73]. Here, a QPSJ based non-destructive readout memory circuit is used as a synapse. The charge capacitor island of Fig. 5(a) is replaced by two series capacitors. The bottom capacitor controls the number of cooper pairs tunneling to the output QPSJ. Therefore, it acts as a synaptic weight for the circuit. Both binary and multistate synaptic memory state has been demonstrated by simple augmentation of the structure [Fig. 5(c)]. These cooper pairs give rise to the output current (I_{out}) of the design.

The power required per switching event of a QPSJ-based neuron is estimated to be $\sim 3.2 \text{ zJ}$ which is much less compared to a JJ-based neuron. Therefore, for a single firing event, a QPSJ-based neuron (with $N=10$ parallel QPSJ and a series QPSJ at the input) dissipates a power equivalent to $\sim 35.2 \text{ zJ}$. The firing speed is estimated to be 10 spikes/ns which implies that the switching time is faster compared to JJ-based neurons. Although a QPSJ-based network has not been experimentally realized yet, it is expected to provide a lower chip area compared to the JJ-based neuromorphic hardware system, because superconducting nanowire has a diameter of several

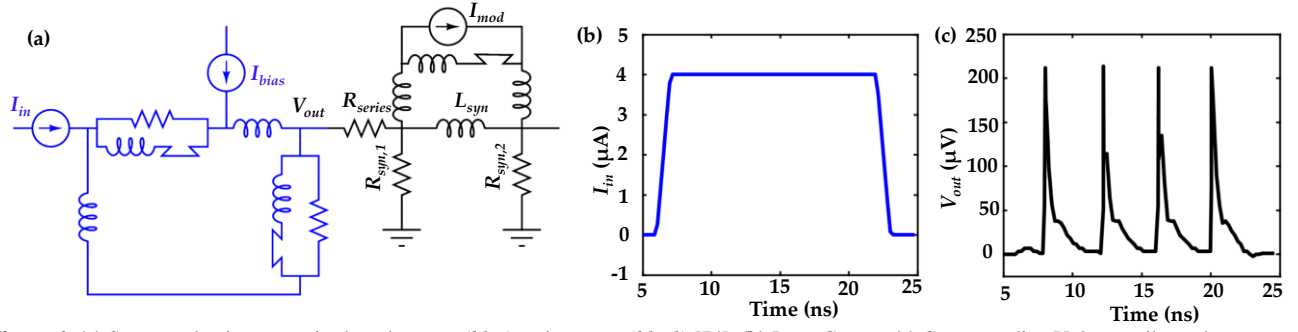


Figure 6: (a) Superconducting nanowire-based neuron (blue) and synapse (black) [74]. (b) Input Current (c) Corresponding Voltage spike at the output

nm only [74]. Although the writing efficiency of the MJJ is high, the process requires an external magnetic field which is not suitable for real-time learning circuit operation. An electrical field tunable QPSJ can give us more flexibility for incorporating QPSJ in neuron and synaptic circuits.

III.A.3. Superconducting Nanowire-based Neuron and Synapse

For a large neuromorphic network, the number of SFQ pulse generated should be high enough to drive large fanout. In this case, JJ has limitations in terms of the number of SFQ pulse generated and for a very large network, So, it can be highly difficult to implement a full neuromorphic network with JJ. Besides, the action potentials in JJ is not strong enough to be detected easily. One possible alternative of JJ can be thin superconducting wire, also known as superconducting nanowire. Superconducting nanowire exhibits switching from superconducting to resistive state and they have been reported to generate a higher number of SFQ pulses as output [72], [73], [75], [76].

In a superconducting nanowire, superconductivity breaks down and the wire turns resistive when the amount of current exceeds a threshold value (I_C), known as the critical current. If the current is decreased below a certain level known as re-trapping current (I_r), the nanowire goes back to the superconducting state [77]. If the nanowire is placed in parallel with a shunt resistance, there will be electrothermal interactions between the nanowire and the shunt resistance, which behaves as a relaxation oscillator. When the current exceeds the critical value, the nanowire turns resistive, and the current abruptly begins to flow through the shunt resistance increasing the voltage across the shunt resistor which decreases the current across the nanowire. At one point the current across the nanowire goes below the re-trapping current (I_r) and the nanowire goes back to the superconducting state. Therefore, the current through the shunt resistance drops and the voltage goes through relaxation.

This hysteretic behavior has been utilized by Toomey *et al.* first to design a superconducting nanowire-based neuron circuit. Here, they proposed a neuron that has the same circuit configuration as the JJ-based neuron proposed by Crotty *et al.* [39]. The interplay between two oscillator circuits generates spiking output voltage [Fig. 6(a)]. Here, a current pulse in input produces pulsating output voltage [Fig. 6(b)]. The bias current (I_{bias}) is chosen such that, the current flowing through both the nanowire is just below the critical value (I_C). When an input

current pulse is given, it is added to the bias current component in the nanowire of the main oscillator. This causes the main oscillator to switch to the resistive state following the injection of a counterclockwise current to the loop. This in turn helps to switch the nanowire of the control oscillator which reduces the counterclockwise current in the loop. This eventually helps the main oscillator to spike again [Fig. 6(c)]. Thus, without the control oscillator, the main oscillator would only be able to fire once. Here, the firing frequency depends on the magnitude of the bias current. The threshold voltage for firing can be set by giving input pulses at the input. A negative pulse sets the threshold voltage low, and a positive pulse does otherwise.

For the connection between neurons, an inductive synapse is introduced between neurons to control the downstream signal. The inductor gets energized by the rapid voltage spikes from the neuron. The effect of the inductive synapse can be excitatory or inhibitory depending on the sign of the bias current applied to the upstream neuron. The synaptic weight/strength can be varied by changing the effective inductance of the synapse. For applying such variability in the inductive synapse, the superconducting nanowire is connected in parallel with the inductor. Since a nanowire's kinetic inductance increases with the increase of bias current, an ideal current source is placed in parallel with the synapse inductor. The overall parallel inductance of the synapse can be modulated by the modulating current I_{mod} . Although this kind of implementation can be suitable for deep learning, this does not capture the true behavior of bio-realistic synapse. The pulse energy is on the order of ~ 10 aJ. The neuron circuit consumes about 0.05 fJ energy for each action potential or firing event (without considering the refrigeration energy), while for the synapse, the energy is around 0.005 fJ. Here, a superconducting transmission line (axon) is also reported, where the neuron signal passed through the axon acquires a delay of 100-500 ps which is the full width of an action potential which is comparatively lower to the mammalian brain (a few ms). Owing to superconducting interconnects, the resistive loss is not present here and the nanowire itself consumes minuscule energy for each action potential generation (~ 0.05 fJ excluding the cooling power). The combination of these two leads to an unprecedented power efficiency. Nanowire-based neuron has been experimentally demonstrated by using thick NbN nanowire with a diameter of 60 nm. The total area of each oscillator is around $10.87 \mu\text{m} \times 8.72 \mu\text{m}$, where most of the area is occupied by a large inductor (around $5.81 \mu\text{m} \times 2.95 \mu\text{m}$). The total area occupied by a single neuron can be estimated to be around $27.17 \mu\text{m} \times 25.64 \mu\text{m}$. The area is promising

considering the fact that a small 9×3 sized network for a simple image recognition task has been reported for image recognition application using the LTspice model of the superconducting nanowire with perfect accuracy [74].

Superconducting nanowire shows superior performance in terms of fanout in a neuromorphic network [74]. JJ and Nanowire both have quantized flux outputs. But nanowire has considerable advantage over JJ in terms of ease of fabrication, CMOS compatibility and scalability. Nanowire permits higher degrees of parallelism compared to JJ and consequently, nanowire permits a higher fanout. In addition to the fanout and fan in, the nanowire output signal has a high magnitude and high duration making it compatible with CMOS control circuitry which gives it an experimental advantage over other superconducting devices. Despite scarce research efforts on superconducting nanowire-based neuromorphic circuits, their promising characteristics call for further exploration.

III.B. Hybrid Superconductor-Semiconductor-based Neuromorphic Hardware.

Since the optical signal propagates at the speed of light, it is intuitive to give effort in building a fast-neuromorphic network based on optical signal [78]. Besides, for optical signal, capacitive and inductive attenuation is not present which further motivates to utilize optical signal for an efficient neuromorphic system. Superconducting nanowire has optical sensitivity for which they are useful in superconductor-based photon detector. Shainline *et al.* first proposed a hybrid semiconductor-superconductor hardware platform where light-emitting diode (LED) with superconducting photonic detector work in combination to behave as a spiking neuron [78]. Optical waveguide connects neurons. Neurons are connected through waveguides that are electromechanically coupled. The distance between two waveguides can be modulated by applying voltage. This gives the coupler a light tunability from 0% to 100% from one waveguide to the other. This coupling strength acts as a synaptic weight which can be modulated through circuit activity. Here a superconducting nanowire single-photon detector (SNSPD) is used to detect photons with high efficiency ($> 90\%$). For detecting and processing optical signals, SNSPD is a natural choice, thanks to its capability of waveguide integration, high speed, and compact size [79], [80].

An SNSPD-based has two components: nanowire detector and LED. Nanowire detectors can sense individual photons [81]. When SNSPDs are connected in parallel with an LED, the detector acts as a photonic signal integrator and this type of detector is referred as parallel nanowire detector (PND). The LED has finite nonzero resistance. When the nanowire detector does not detect a photon, it remains superconducting. For a PND, if any of the branches remain superconducting, then all the bias current passes through the nanowire branches. When all the detectors in a PND detect photons, they all turn resistive. Consequently, the bias current exceeds the critical current of the PND, and biasing current is redirected through the LED generating a light signal. This light signal is propagated through the waveguides to the subsequent neurons. It is also possible to connect two SNSPDs in series so that absorption in one of the nanowires, decreases the firing threshold of another one. In such a network, absorption in the upstream nanowire decreases

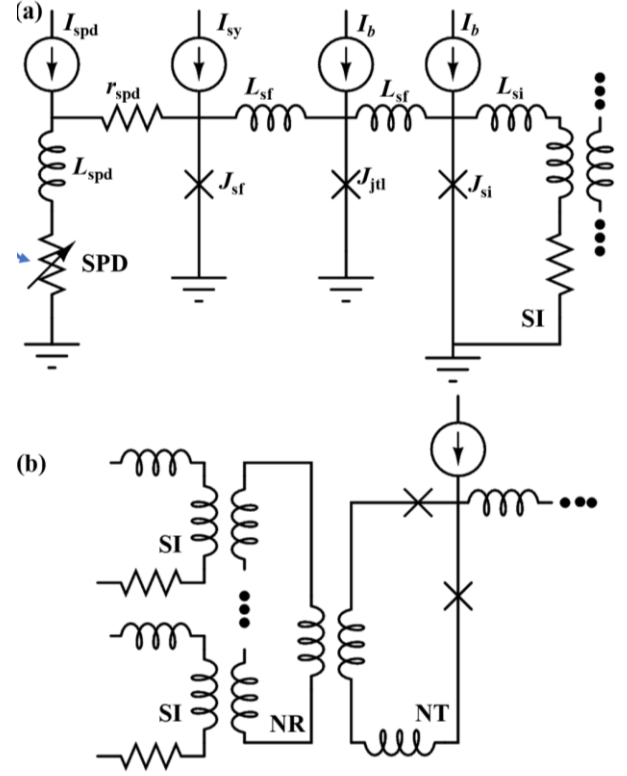


Figure 7: (a) Circuit diagram of a photon to fluxon transducer. (b) Circuit diagram of multiple synapses (SI loops) connected to the NR loop and the neuronal thresholding (NT) loop through mutual inductors [84].

the current flowing through the branch and thus more photons are required to be absorbed by another nanowire connected in series [82].

It is possible to decouple the firing threshold and LED gain by introducing a cryotron device. There are two types of cryotron devices, nano cryotron (nTron) and heater cryotron (hTron). The nTron is a three-terminal device that works as a switch by the joule heating process. When the gate current of an nTron exceeds a critical current, the path from source to drain becomes resistive. If connected with a load parallelly, the current is bypassed through it. Shainline *et al.* utilized this characteristic to drive the output LED to be driven by a certain bias current [78]. Individual neurons are connected through optical waveguides. Optical waveguides have distinct advantages over electrical connection because it allows individual neurons to collect and integrate optical signal from many neurons and integrate them without time-multiplexing [83]. Here, a stingray neuron is proposed where each neuron combines the modes from a large number of waveguides without significant loss via a landing pad containing the PND arrays. Hundreds of waveguides are combined in a receiver body with less than 0.2 dB insertion loss from any port.

For synaptic weight, here an electromechanically actuated waveguide couplers are proposed as the synaptic weight for the network. The coupling can be varied by varying the distance between the waveguides electromechanically by applying voltage. The maximum distance (minimum coupling) occurs at 0 V between the two waveguides. Upon activity, a voltage difference is created between the two waveguides which increases the coupling strength. Spike Timing Dependent

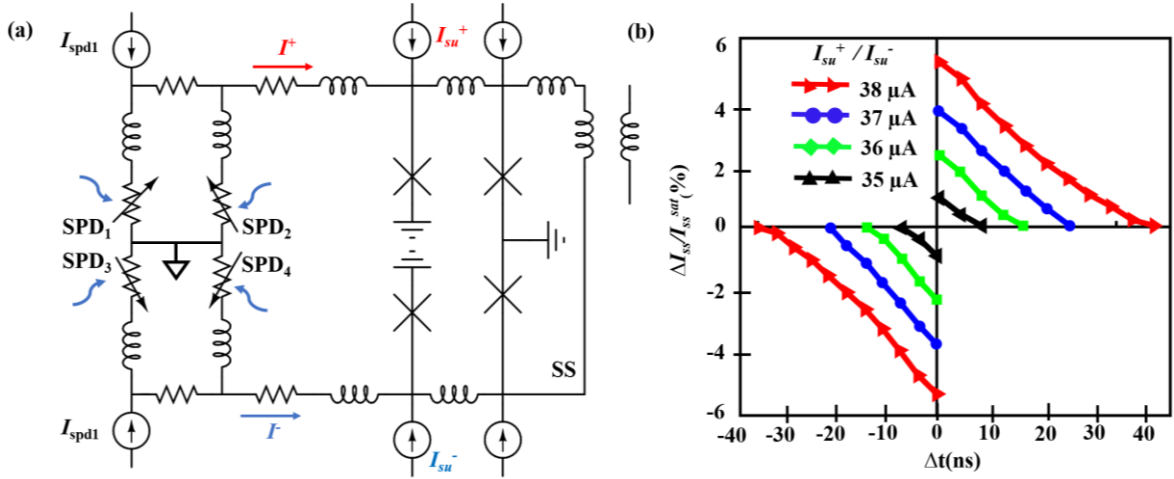


Figure 8: (a) Implementation of spike-timing-dependent plasticity. (a) Circuit under consideration [84]. (b) Change in current stored in the SS loop as a percentage of the total storage capacity of the loop vs the relative arrival time of the two photons involved, Δt .

Plasticity (STDP) can be implemented if closely spaced firing events from upstream and downstream neurons place charge on the capacitor.

There are three primary sources of energy dissipation in this design, the inductive energy of supercurrent flowing through the circuit, the capacitive energy of the LED, and the energy required to produce the photons. Here the energy required for each photon generation depends on the LED efficiency. Most of the energy is consumed in supplying current to the inductors and charging the capacitors. At unity efficiency, the energy required is 2 aJ/photon while for 1% efficiency the energy becomes 20 aJ/photon which is much smaller compared to CMOS-based neuron. Thus, the use of a hybrid platform of superconducting electronics and optoelectronics offers a factor of 10^6 improvements in energy efficiency compared to the best-performing CMOS process available.

In a subsequent work, Shainline *et al.* proposed superconducting optoelectronic loop-based neurons [84] (Fig. 7). Here, light is used to communicate between neurons, and synaptic weight is implemented in the electric domain. A neuron with a single integration loop can receive input from thousands of synaptic connections. In this work, a superconducting photonic detector is used in conjunction with a JJ to detect photons and then integrate this current through a synaptic loop [85]. With a single photon detection, the single-photon detector transduces the photon to an electrical current. The current through the JJ exceeds the critical current and produces flux pulses known as fluxons. Here, fluxons are voltage spikes across the synaptic JJ. These fluxons are integrated as the current in the Synaptic integration loop. The neuronal receiving (NR) loop integrates the current that it receives from all the neuron's synapses.

In this design, the use of mutual inductors allows many synapses to be connected with one neuron and add current to the neuronal receiving loop without any current leakage path. Finally, the NR loop is connected to a larger loop referred to as Neuronal Thresholding (NT) loop. The NT loop works as a transformer that steps up the current to be detected beyond the threshold value. Here the fluxons are referred to as synaptic firing events. The number of synaptic firing events can be controlled by a current biased JJ (J_{sf}). The critical current of J_{sf}

can be varied by a current bias and it can control the number of fluxons that are created. For low critical current, the SPD current is higher than the critical current for a long duration and thus it creates a large number of fluxons. If the critical current is higher, the number of fluxons is lower. This critical current is the synaptic weight for this circuit. Excitatory and inhibitory connections between upstream and downstream neurons have also been theoretically reported by choosing the sign of mutual coupling between the Synaptic Integration (SI) loop and Neuronal Receiving (NR) loop [84].

The synaptic current (I_{sy}) can be dynamically varied to vary the synaptic strength of the learning circuit. Shainline *et al.* reported variable synaptic strength for both supervised and unsupervised learning for this circuit configuration [78]. To implement supervised learning, two additional control pulses are used which (I^+/I^-) can turn the synapse into either potentiation or depression state of operation (Fig. 8(a)). For modulating the synaptic weight in smaller steps, a superconducting loop that is capable of storing multiple fluxons is also reported. Here a DC-to-SFQ converter is used to add flux quanta one by one. Two separate biasing signals I^+ and I^- can drive the synapse to either potentiation or depression by adding fluxons in opposite directions [84].

The Hebbian learning rule is also implemented by implementing two correlated detection schemes. When a correlated SNSPD detects photon from post-neuron within a certain time after the pre-neuron fires, a current is injected into the synaptic storage loop. The amount of current that is injected into the synaptic storage loop depends on the time difference between the pre-neuron and post-neuron firing. Spike-timing dependent plasticity (STDP) based learning is also reported by mirroring the Hebbian learning circuit for a current injection in the SS loop from the opposite direction. Here, synaptic depression occurs when the presynaptic neuron fires later than the post-synaptic neuron [Fig. 8(b)] [86]. When a photon is detected in the pre-neuron detector closely followed by a photon detection in the post neuron, I_{spd1} is diverted to the SS loop to increase the injected current in the clockwise direction and thereby increasing the synaptic weight. In the mirror circuit, SPD3 and SPD4 detect photons from post-neuron and pre-neuron respectively. Consequently, when the post neuron fires

a photon before pre-neuron, a current is injected in the SS loop in the counterclockwise direction and this pushes the current in the counterclockwise direction, which decreases the synaptic weight. Thus, the synaptic weight can be modified by the timing difference of pre-neuron and post-neuron firing. The Synaptic storage loop is coupled with the synaptic biasing loop which determines the biasing current of the synapse. The biasing current is used to inject current in the synaptic integration loop which is coupled to the neuronal thresholding loop. Current from the neuronal thresholding loop is sent to the cryotron-based transmitter circuit to produce an optical signal via LED.

Large scale theoretical demonstration of superconducting-optoelectronic neuromorphic hardware platform has been reported and the energy and area specifications show promising prospect [84]. The switching energy for an SNSPD is reported to be 21 zJ. The power consumption is 1 mW for a network with 8100 neurons and the total on-chip power is less than 10 mW which includes the power consumed by the biasing currents [84]. The reported area of a network with 8100 neurons including three different pairs of waveguide routing is about 1cm^2 . The overall area of such a network depends on the degree of interconnectivity nodes. Although, the inductor in the SI and SS loop is reported to have a value $1\text{ }\mu\text{H}$ with an area of $5 \times 5\text{ }\mu\text{m}^2$, the most area consuming component of the neuron is the

driver amplifier for LED and mutual inductance. But the overall area is mostly dictated by the passive waveguide requirement. In this platform, a system with 10^6 neurons and 200×10^6 synapses on a 300 mm wafer consumes 1 W of power including the cooling power. This energy specification indicates that this platform is very promising in large-scale network implementation. The network offer tunability of synaptic weight, neuronal threshold, firing frequency and can implement STDP based learning rule via the current biasing scheme. Table II summarizes the relative comparison of the fan-in and fan-out capacity of different superconducting neuromorphic devices. Because optical interconnect has no resistance, capacitance, or inductance, they can provide massive fanout capacity as is reflected in Table II. The hybrid semiconductor-superconductor platform, therefore, has a better fan-in and fan-out capacity, and consequently a higher parallelism capability compared to the superconductor-based neuromorphic devices.

III.C. Non-Superconducting Cryogenic Materials

Several materials which have switching behavior in normal temperature, have been reported to maintain their characteristics in cryogenic temperature. Hence, they were explored for neurosynaptic behavior in cryogenic temperature. Certain underlying physics can be attributed for the switching behavior in these materials. For example, nonlinear transport mechanisms, Mott transition have engendered unique advantages in NbO_x -based material [87], [88]. A simple structure of a Pt- NbO_2 -Pt is shown in figure 9(a). When a sufficient voltage is applied in NbO_2 -based device, the resistivity changes from the insulating state to the metallic state. This switching behavior manifests hysteresis in its I-V characteristics which has been utilized in designing novel neuromorphic circuit [Fig. 9(b)].

III.C.1. Threshold switching-based neuron

Several oxides (HfO_2 , VO_2 , NbO_2) have been reported to exhibit metal to insulator transition and abrupt switching characteristics in low temperatures. Fang *et al.* have analyzed the cryogenic behavior of HfO_x based synapse and demonstrated that HfO_x can maintain its switching behavior at 4K [89]. Both R_{HRS} and R_{LRS} decrease with increasing temperature in the case of a Pt/ HfO_x /TiN structure and high $R_{\text{HRS}}/R_{\text{LRS}}$ is observed for low temperature which is a potential requirement for RRAM based synapse.

When NbO_x is connected with an external resistor, the voltage across the NbO_x (membrane voltage) starts to self-oscillate, and here the oscillation frequency is proportional to the conductance [Fig. 9(d)]. For an RRAM connected in series with it, the oscillation frequency is proportional to RRAM conductance and therefore it is feasible for integrating the weighted sum current in a crossbar synaptic array [Fig. 9(c)]. NbO_2 manifests hysteretic behavior within a large range of temperature and therefore, has potential application in cryogenic neuromorphic hardware [Fig. 9(f)]. Wang *et al.* have proposed a NbO_2 based oscillatory neuron in series with previously proposed HfO_x based cryogenic RRAM-based synapse [42]. They demonstrated that NbO_2 maintains its hysteretic behavior at a very low temperature [Fig. 9(e)].

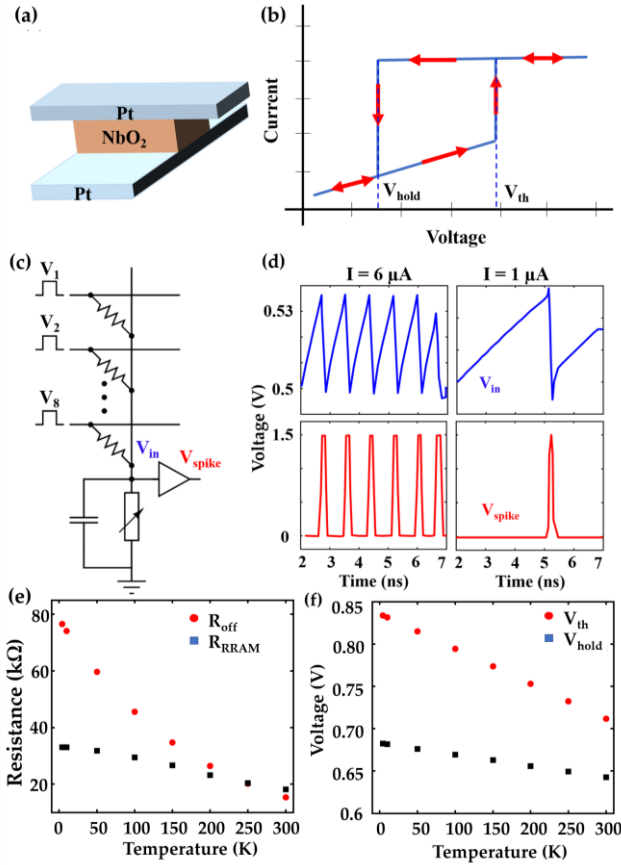


Figure 9 (a) A Pt- NbO_2 -Pt device with its (b) I-V characteristics (c) Proposed design of an oscillation neuron with a MIT device at the end of the column that emulates the V_{in} node [54]. (d) The waveform of the CMOS integrate-and-fire neuron for different weighted sum current values (6 μA vs. 1 μA). (e) variation of RRAM resistance and off-resistance with temperature. (f) Threshold voltage (V_{th}) and hold.voltage (V_{hold}) variation with temperature.

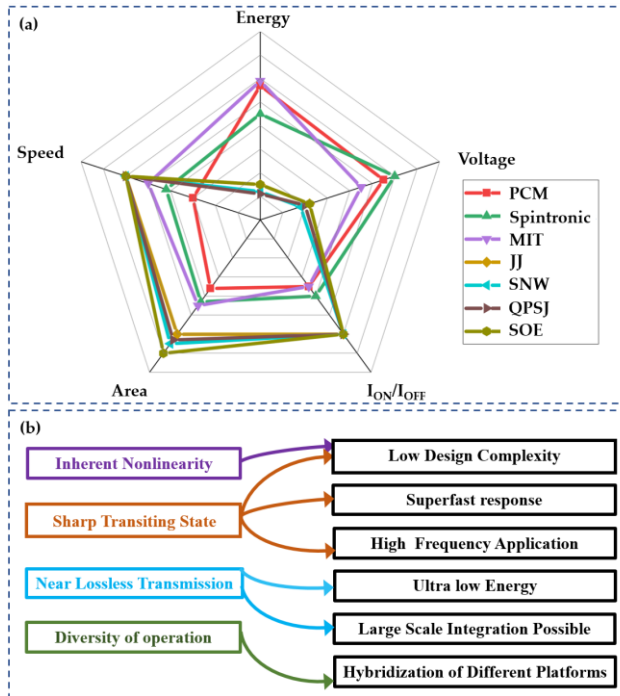


Figure 10: (a) Comparison of different existing hardware platforms and a few cryogenic hardware platforms on five different metrics. (b) Properties of Cryogenic devices and their advantages for utilizing neuromorphic hardware.

Beyond a threshold voltage (V_{th}), it switches to a low resistive state, and below a certain voltage (V_{hold}), it retains its high resistive state [Fig. 9(b)]. When a voltage is applied, the parasitic capacitance C_1 gets charged by the voltage across NbO_2 . If the voltage is greater than the threshold voltage, then it switches to a low resistance state (R_{ON}). Now if the voltage across the neuron is less than V_{hold} , then the neuron goes back to a high resistive state, and C_1 is discharged. This way the neuron oscillates between the two voltage levels, V_{th} and V_{hold} . From the temperature frequency analysis, it is seen that, even though the oscillation frequency increases with temperature, the oscillation frequency at an ultra-low temperature (4 K) is still in the GHz range.

Chen *et al.* has conducted a comprehensive analysis to derive a performance control method of the oscillation behavior of NbO_2 based device very recently [30]. In this Pt- NbO_x -TiN based device, a threshold switch is fabricated. The NbO_x layer is divided into two parts, NbO_2 based switching layer and a conducting layer of Nb_2O_5 . If the temperature decreases, both V_{th} and V_{hold} increase. But V_{th} increases more than V_{hold} [Fig. 9(f)]. So, an expansion of the hysteresis loop occurs with the decrease of temperature. Besides, as the temperature decreases, both the switching time and thermal conductivity increase. Switching time is another way by which we can modulate the oscillation frequency. Oscillation frequency decreases with switching time and the higher the threshold voltage is, the oscillation frequency is lower for a particular switching time. It is evident that at low-temperature NbO_2 exhibits high R_{OFF} and therefore superior performance. The higher the threshold voltage is, the oscillation frequency is lower for a particular switching time. The fabricated Pt- NbO_x -Pt device has an active area of $10 \times 10 \mu m^2$ in a cross-point architecture. This is 12.5 times smaller than the equivalent CMOS based architecture

area [90]. It is evident that at low-temperature NbO_2 exhibits high R_{OFF} and therefore superior performance. Figure 10(b) summarizes the characteristics of the different cryogenic platforms and their broader advantages.

IV. Comparative Study

In previous sections, we have discussed state-of-the-art cryogenic memory devices. In this section, we compare them based on energy consumption, spike generation rate and several other metrics. The existing neuromorphic platforms such as CMOS-based, memristor-based, PCM-based, Spin-based, FeFET-based are technologically more mature than cryogenic neuromorphic hardware. Some CMOS-based digital implementation of neuromorphic chips have already been fabricated by Intel and IBM[91], [92]. However, the design requirement is still strenuous, and the power consumption is still far beyond the power consumed by the biological counterpart. Although there exists a power disadvantage of the cryogenic environment in cryogenic neuromorphic hardware, the intrinsic power consumption is still far below than conventional platforms. The resistive interconnects lead to supply voltage degradation and self-heating in a conventional crossbar-based synaptic network. On the contrary, dissipation less superconducting interconnects in cryogenic temperature provide a pathway to curb the interconnect loss. Still, much more research is still required for superconducting interconnect to match the massive parallelism of biological brain. Besides, most of the cryogenic devices are based on superconducting entities (JJ, QPSJ, Superconducting Nanowire). JJ-based neurons and synapses operate at μV range. Due to low operating voltage, JJ-based neurons consume several attojoules (aJ) of power intrinsically. Even with the additional energy required for cooling, the overall power consumption remains orders of magnitude lower than the conventional platforms [93]. Another important aspect of the neuromorphic system, which is mostly out of the scope of this review, is the design of analog to digital conversion (ADC) blocks. ADCs are known to be the most power-hungry and area consuming modules in conventional crossbar-based neuromorphic systems. The possibilities of (i) designing specialized area-efficient cryogenic ADCs or (ii) to avert the need for ADCs by implementing a fully analog neuromorphic system are yet to be thoroughly tested/validated. There have been several reports on superconducting ADCs with promising figures-of-merit [94]–[96]. However, this is still an evolving field of research and there is a strong need for further exploration.

For QPSJ-based neurons and synapses, the power consumption is comparatively much lower (several zJ). QPSJ-based multi-state synapse has also been theoretically proposed which consumes zJ range of power. The spiking rate is also on the order of 10^{10} for QPSJ based neurons. For nanowire-based neurons, the power consumption is reported to be 0.05 fJ. The nanowire-based neurons are capable of a high fanout network due to the production of a massive amount of flux quanta. Although optoelectronic-based neurons and synapses require semiconductor and superconductor hybrid implementation, they are capable of faster communication between neurons and synapses because they transmit signals at the speed of light. Due

Table III: Comparison of different cryogenic neuromorphic hardware platform.

Device Type	Structure	Operating Voltage	Temperature	Number of States	Firing Energy	Spikes per second	Ref.
Josephson Junction Based	JJ (Nb/Mn/Nb/SiO ₂) as synapse	150 μ V	4 K	Number of I_c of MJJ	150 zJ (SFQ pulse energy)	1.6 $\times 10^9$ spikes per second(est.)	Schneider et.al., 2017 [62]
Quantum Phase Slip Junction (QPSJ) based	Mo-Ge deposited on suspended carbon nanotubes	1mV	<1.92 K	Both binary and multiple states are possible. Modulated by critical voltage of QPSJ (Cheng <i>et. al.</i> , 2021)	6.4 zJ (switching energy \times N)	2 $\times 10^{10}$ spikes per second (estimated)	Cheng et.al., 2018 [72]
Superconducting Nanowire Based	NbN/SiO _x	250 μ V(est.)	4.2 K	Depends on the number of the modulating current bias	50 aJ (switching energy)	0.25 $\times 10^9$ spikes per second(est.)	Toomey et.al.,2019 [75] Toomey et.al.,2020 [74]
SNSPD based Neuron	NbN nanowire as SNSPD, NbN on GaAs substrate as waveguide.	-----	2 K	Multiple	20 aJ / photon 20 fJ / photon (including cooling)	10 ¹⁵ synaptic event per second	Shainline et.al.,2017 [78]
Superconducting Optoelectronic Loop Neuron	NbN nanowire as SPD	>0.1V for LED to generate photon (Shainline et.al.,2017)	4.2 K	Multiple (a few hundred)	2.7 aJ (weak synaptic efficacy) 41aJ (strong synaptic efficacy)	10 ¹⁵ synaptic event per second	Shainline et.al. 2019 [84]
Pt/NbOx/TiN device	Pt/NbOx/TiN on TiN/ SiO ₂ / Si substrate	2V	100K-300K reproted	Binary (RRAM)	-----	Spiking rate Depends on Temperature (~14 $\times 10^6$ to ~7 $\times 10^6$)	Chen et.al.,2021[30]

to the high number of synaptic events, they can send a high degree of parallelism.

Finally, NbO₂ based neuron is promising for their natural oscillatory behavior, temperature-dependent spiking rates and a wide range of operating temperature. Efforts have also been given to utilize the advantages of several devices by combining them in a single circuit Table III summarizes the overall performance comparison of the state-of-the-art cryogenic neuromorphic hardware base.

V. Conclusion

With the ongoing pursuit of artificial intelligence hardware, neuromorphic architecture is the most promising among them due to its massive parallelism. But the power efficiency and speed are still far below the human brain. Due to the design complexity and power requirement of conventional neuromorphic hardware in current neuromorphic devices, it is imperative to study cryogenic neuromorphic hardware for designing a neuromorphic network with superior performance. In this review, we have carefully classified the existing neuromorphic devices and discussed their advantages and disadvantages in brief. Although there are cryogenic versions of conventional CMOS devices, they suffer from performance degradation in ultralow temperature and possess design complexity [97]. The energy consumption of a superconducting processor prototype has been proved to be ~80X less than that of its semiconductor counterpart(considering cooling cost) [98]. Superconducting devices suffer from scalability issue due to the coherence length (~200-700nm) constraints and large size. On the other hand CMOS technology is highly mature and scalable. Nevertheless, superconducting electronics offer excellent speed and power consumption performance comparative to the conventional hardware [99]–[101]. Figure

10(a) shows a relative comparison of some cryogenic devices with a few leading conventional platforms for implementing neuromorphic hardware. Figure 10(b) shows several properties of cryogenic device platforms and their corresponding advantages in a neuromorphic network. It is evident that, cryogenic platforms are superior to the conventional platforms in several important metrics of performance. Undoubtedly, it is in our best interest to prepare ourselves for further exploration of cryogenic neuromorphic hardware

References

- [1] A. A. Chien and V. Karamcheti, "Moore's law: The first ending and a new beginning," *Computer*. 2013, doi: 10.1109/MC.2013.431.
- [2] B. Bailey, "The Impact of Moore's Law Ending," *Semiconductor Engineering*, 2018. .
- [3] N. Shah, "Moore's Law is Ending: What's Next After FinFETs," 2021, doi: 10.1007/978-3-030-63089-8_22.
- [4] E. Masanet, A. Shehabi, N. Lei, S. Smith, and J. Koomey, "Recalibrating global data center energy-use estimates," *Science* (80-.), 2020, doi: 10.1126/science.aba3758.
- [5] A. Bogdanov *et al.*, "Analog-digital approach in human brain modeling," 2017, doi: 10.1109/CCGRID.2017.91.
- [6] S. X. Moffett, S. M. O'Malley, S. Man, D. Hong, and J. V. Martin, "Dynamics of high frequency brain activity," *Sci. Rep.*, 2017, doi: 10.1038/s41598-017-15966-6.
- [7] I. Chakraborty, A. Jaiswal, A. K. Saha, S. K. Gupta, and K. Roy, "Pathways to efficient neuromorphic computing with non-volatile memory technologies," *Applied Physics Reviews*. 2020, doi: 10.1063/1.5113536.
- [8] E. M. Izhikevich, "Simple model of spiking neurons," *IEEE Transactions on Neural Networks*. 2003, doi: 10.1109/TNN.2003.820440.
- [9] W. Maass, "Networks of spiking neurons: The third generation of neural network models," *Neural Networks*, 1997, doi: 10.1016/S0893-6080(97)00011-7.
- [10] A. Tavanaei, M. Ghodrati, S. R. Kheradpisheh, T. Masquelier, and A. Maida, "Deep learning in spiking neural networks," *Neural Networks*. 2019, doi: 10.1016/j.neunet.2018.12.002.

- [11] X. Wang, X. Lin, and X. Dang, "Supervised learning in spiking neural networks: A review of algorithms and evaluations," *Neural Networks*, 2020, doi: 10.1016/j.neunet.2020.02.011.
- [12] J. L. Lobo, J. Del Ser, A. Bifet, and N. Kasabov, "Spiking Neural Networks and online learning: An overview and perspectives," *Neural Networks*, 2020, doi: 10.1016/j.neunet.2019.09.004.
- [13] H. S. Choi *et al.*, "3-D floating-gate synapse array with spike-time-dependent plasticity," *IEEE Trans. Electron Devices*, 2018, doi: 10.1109/TED.2017.2775233.
- [14] M. Prezioso, F. Merrih Bayat, B. Hoskins, K. Likharev, and D. Strukov, "Self-Adaptive Spike-Time-Dependent Plasticity of Metal-Oxide Memristors," *Sci. Rep.*, 2016, doi: 10.1038/srep21331.
- [15] R. Gopalakrishnan and A. Basu, "Triplet Spike Time-Dependent Plasticity in a Floating-Gate Synapse," *IEEE Trans. Neural Networks Learn. Syst.*, 2017, doi: 10.1109/TNNLS.2015.2506740.
- [16] A. Sengupta, A. Banerjee, and K. Roy, "Hybrid Spintronic-CMOS Spiking Neural Network with On-Chip Learning: Devices, Circuits, and Systems," *Phys. Rev. Appl.*, 2016, doi: 10.1103/PhysRevApplied.6.064003.
- [17] D. Ma *et al.*, "Darwin: A neuromorphic hardware co-processor based on spiking neural networks," *J. Syst. Archit.*, 2017, doi: 10.1016/j.sysarc.2017.01.003.
- [18] A. R. Young, M. Dean, J. S. Plank, and G. S. Rose, "A Review of spiking neuromorphic hardware communication systems," *IEEE Access*, 2019, doi: 10.1109/ACCESS.2019.2941772.
- [19] T. Gonzalez-Raya, X. H. Cheng, I. L. Egusquiza, X. Chen, M. Sanz, and E. Solano, "Quantized Single-Ion-Channel Hodgkin-Huxley Model for Quantum Neurons," *Phys. Rev. Appl.*, vol. 12, no. 1, p. 1, 2019, doi: 10.1103/PhysRevApplied.12.014037.
- [20] L. Xia *et al.*, "MNSIM: Simulation Platform for Memristor-Based Neuromorphic Computing System," *IEEE Trans. Comput. Des. Integr. Circuits Syst.*, 2018, doi: 10.1109/TCAD.2017.2729466.
- [21] M. A. Zidan, J. P. Strachan, and W. D. Lu, "The future of electronics based on memristive systems," *Nat. Electron.*, 2018, doi: 10.1038/s41928-017-0006-8.
- [22] B. Yan, Y. Chen, and H. Li, "Challenges of memristor based neuromorphic computing system," *Sci. China Inf. Sci.*, 2018, doi: 10.1007/s11432-017-9378-3.
- [23] C. Sung, H. Hwang, and I. K. Yoo, "Perspective: A review on memristive hardware for neuromorphic computation," *J. Appl. Phys.*, 2018, doi: 10.1063/1.5037835.
- [24] J. Hong *et al.*, "A Dual Magnetic Tunnel Junction-Based Neuromorphic Device," *Adv. Intell. Syst.*, 2020, doi: 10.1002/aisy.202070120.
- [25] J. Cai *et al.*, "Voltage-Controlled Spintronic Stochastic Neuron Based on a Magnetic Tunnel Junction," *Phys. Rev. Appl.*, 2019, doi: 10.1103/PhysRevApplied.11.034015.
- [26] J. Torreon *et al.*, "Neuromorphic computing with nanoscale spintronic oscillators," *Nature*, 2017, doi: 10.1038/nature23011.
- [27] J. Singh, "Implementation of Memristor Towards Better Hardware/Software Security Design," *Transactions on Electrical and Electronic Materials*. 2021, doi: 10.1007/s42341-020-00269-x.
- [28] J. Zhu, T. Zhang, Y. Yang, and R. Huang, "A comprehensive review on emerging artificial neuromorphic devices," *Applied Physics Reviews*. 2020, doi: 10.1063/1.5118217.
- [29] C. Hutter, E. A. Tholén, K. Stannigel, J. Lidmar, and D. B. Haviland, "Josephson junction transmission lines as tunable artificial crystals," *Phys. Rev. B - Condens. Matter Mater. Phys.*, 2011, doi: 10.1103/PhysRevB.83.014511.
- [30] A. Chen *et al.*, "Comprehensive regulation of the threshold oscillation for neuromorphic systems based on cryogenic performance of NbO₂ device," *IEEE Electron Device Lett.*, vol. 42, no. 5, pp. 692–695, 2021, doi: 10.1109/LED.2021.3068823.
- [31] T. Yamazaki, J. Igarashi, and H. Yamaura, "Human-scale Brain Simulation via Supercomputer: A Case Study on the Cerebellum," *Neuroscience*. 2021, doi: 10.1016/j.neuroscience.2021.01.014.
- [32] A. Parent and M. B. Carpenter, "Carpenter's human neuroanatomy," p. 1011, 1996.
- [33] P. J. Harrison, N. Freemantle, and J. R. Geddes, "Meta-analysis of brain weight in schizophrenia," *Schizophr. Res.*, 2003, doi: 10.1016/S0920-9964(02)00502-9.
- [34] K. P. Cosgrove, C. M. Mazure, and J. K. Staley, "Evolving Knowledge of Sex Differences in Brain Structure, Function, and Chemistry," *Biological Psychiatry*. 2007, doi: 10.1016/j.biopsych.2007.03.001.
- [35] E. Miranda and J. Suñé, "Memristors for neuromorphic circuits and artificial intelligence applications," *Materials*. 2020, doi: 10.3390/ma13040938.
- [36] J. Wu, Y. Chua, and H. Li, "A Biologically Plausible Speech Recognition Framework Based on Spiking Neural Networks," 2018, doi: 10.1109/IJCNN.2018.8489535.
- [37] R. Yang, H. M. Huang, and X. Guo, "Memristive Synapses and Neurons for Bioinspired Computing," *Advanced Electronic Materials*. 2019, doi: 10.1002/aelm.201900287.
- [38] "Biorealistic spiking neural network on FPGA," 2013, doi: 10.1109/ciss.2013.6616689.
- [39] P. Crotty, D. Schult, and K. Segall, "Josephson junction simulation of neurons," *Phys. Rev. E - Stat. Nonlinear, Soft Matter Phys.*, vol. 82, no. 1, pp. 1–8, 2010, doi: 10.1103/PhysRevE.82.011914.
- [40] J. Vista and A. Ranjan, "A simple floating mos-memristor for high-frequency applications," *IEEE Trans. Very Large Scale Integr. Syst.*, 2019, doi: 10.1109/TVLSI.2018.2890591.
- [41] P. A. Merolla *et al.*, "A million spiking-neuron integrated circuit with a scalable communication network and interface," *Science (80-.)*, 2014, doi: 10.1126/science.1254642.
- [42] D. S. Modha *et al.*, "A million spiking-neuron integrated circuit with a scalable communication network and interface," *Science (80-.)*, 2014.
- [43] J. Hasler and B. Marr, "Finding a roadmap to achieve large neuromorphic hardware systems," *Front. Neurosci.*, 2013, doi: 10.3389/fnins.2013.00118.
- [44] W. F. Clark, B. El-Kareh, R. G. Pires, S. L. Titcomb, and R. L. Anderson, "Low Temperature CMOS—A Brief Review," *IEEE Trans. Components, Hybrids, Manuf. Technol.*, 1992, doi: 10.1109/33.148509.
- [45] J. Grollier, D. Querlioz, K. Y. Camsari, K. Everschor-Sitte, S. Fukami, and M. D. Stiles, "Neuromorphic spintronics," *Nature Electronics*. 2020, doi: 10.1038/s41928-019-0360-9.
- [46] Y. Beiliard, F. Paquette, F. Brousseau, S. Ecoffey, F. Alibart, and D. Drouin, "Investigation of resistive switching and transport mechanisms of Al₂O₃/TiO₂-x memristors under cryogenic conditions (1.5 K)," *AIP Adv.*, 2020, doi: 10.1063/1.5140994.
- [47] S. Lashkare, S. Chouhan, T. Chavan, A. Bhat, P. Kumbhare, and U. Ganguly, "PCMO RRAM for Integrate-and-Fire Neuron in Spiking Neural Networks," *IEEE Electron Device Lett.*, 2018, doi: 10.1109/LED.2018.2805822.
- [48] S. Park *et al.*, "Neuromorphic speech systems using advanced ReRAM-based synapse," 2013, doi: 10.1109/IEDM.2013.6724692.
- [49] K. K. Likharev and J. Lukens, "Dynamics of Josephson Junctions and Circuits," *Phys. Today*, 1988, doi: 10.1063/1.2811641.
- [50] K. Y. Arutyunov and J. S. Lehtinen, "Quantum Phase Slip as a Dual Process to Josephson Tunneling," 2019, doi: 10.1088/1742-6596/1190/1/012003.
- [51] J. S. Lehtinen, K. Zakharov, and K. Y. Arutyunov, "Coulomb blockade and bloch oscillations in superconducting Ti nanowires," *Phys. Rev. Lett.*, 2012, doi: 10.1103/PhysRevLett.109.187001.
- [52] "Introduction to the dynamics of Josephson junctions - NASA/ADS," <https://ui.adsabs.harvard.edu/abs/1985MoIzN....Q....L/abstract> (accessed Mar. 22, 2022).
- [53] P. Wang, A. I. Khan, and S. Yu, "Cryogenic behavior of NbO₂ based threshold switching devices as oscillation neurons," *Appl. Phys. Lett.*, vol. 116, no. 16, p. 162108, 2020, doi: 10.1063/5.0006467.
- [54] D. Marković and J. Grollier, "Quantum neuromorphic computing," *Appl. Phys. Lett.*, vol. 117, no. 15, 2020, doi: 10.1063/5.0020014.
- [55] M. J. Deen, "Digital Characteristics of CMOS Devices at Cryogenic Temperatures," *IEEE J. Solid-State Circuits*, 1989, doi: 10.1109/4.16315.
- [56] D. Marković, A. Mizrahi, D. Querlioz, and J. Grollier, "Physics for neuromorphic computing," *Nature Reviews Physics*. 2020, doi: 10.1038/s42254-020-0208-2.
- [57] K. Das, "Low Temperature Microelectronics Design for Digital Readout of Single Electron Transistor Electrometry," *Fac. Eng. Sch. Electr. Eng. Telecommun.*, 2013.
- [58] M. L. Schneider, C. A. Donnelly, and S. E. Russek, "Tutorial: High-speed low-power neuromorphic systems based on magnetic Josephson junctions," *J. Appl. Phys.*, vol. 124, no. 16, 2018, doi: 10.1063/1.5042425.

- [59] R. L. Kautz, "Picosecond pulses on superconducting striplines," *J. Appl. Phys.*, 1978, doi: 10.1063/1.324387.
- [60] B. D. Josephson, "Possible new effects in superconductive tunnelling," *Phys. Lett.*, 1962, doi: 10.1016/0031-9163(62)91369-0.
- [61] T. Li, J. Gallop, L. Hao, and E. Romans, "Ballistic Josephson junctions based on CVD graphene," *Supercond. Sci. Technol.*, 2018, doi: 10.1088/1361-6668/aaab81.
- [62] M. L. Schneide *et al.*, "Energy-efficient single-flux-quantumbased neuromorphic computing," *2017 IEEE Int. Conf. Rebooting Comput. ICRC 2017 - Proc.*, vol. 2017-Janua, pp. 1–4, 2017, doi: 10.1109/ICRC.2017.8123634.
- [63] M. L. Schneider *et al.*, "APPLIED SCIENCES AND ENGINEERING Ultralow power artificial synapses using nanotextured magnetic Josephson junctions," 2018, [Online]. Available: <http://advances.sciencemag.org/>.
- [64] M. L. Schneider *et al.*, "Synaptic weighting in single flux quantum neuromorphic computing," *Sci. Rep.*, 2020, doi: 10.1038/s41598-020-57892-0.
- [65] U. S. Goteti and R. C. Dynes, "Superconducting neural networks with disordered Josephson junction array synaptic networks and leaky integrate-and-fire loop neurons," *J. Appl. Phys.*, vol. 129, no. 7, 2021, doi: 10.1063/5.0027997.
- [66] M. L. Schneider and K. Segall, "Fan-out and fan-in properties of superconducting neuromorphic circuits," *J. Appl. Phys.*, vol. 128, no. 21, 2020, doi: 10.1063/5.0025168.
- [67] I. Burman, A. Hore, A. Chakraborty, S. Bandyopadhyay, and S. Chakrabarti, "Implementation of a Spiking Neuron in CMOS," 2021, doi: 10.1109/ncc52529.2021.9530104.
- [68] O. V. Astafiev *et al.*, "Coherent quantum phase slip," *Nature*, 2012, doi: 10.1038/nature10930.
- [69] J. E. Mooij and Y. V. Nazarov, "Superconducting nanowires as quantum phase-slip junctions," *Nat. Phys.*, 2006, doi: 10.1038/nphys234.
- [70] N. Giordano, "Evidence for macroscopic quantum tunneling in one-dimensional superconductors," *Phys. Rev. Lett.*, 1988, doi: 10.1103/PhysRevLett.61.2137.
- [71] U. S. Goteti and M. C. Hamilton, "SPICE model implementation of quantum phase-slip junctions," *Electron. Lett.*, 2015, doi: 10.1049/el.2015.0904.
- [72] R. Cheng, U. S. Goteti, and M. C. Hamilton, "Spiking neuron circuits using superconducting quantum phase-slip junctions," *J. Appl. Phys.*, vol. 124, no. 15, 2018, doi: 10.1063/1.5042421.
- [73] R. Cheng, U. S. Goteti, and M. C. Hamilton, "High-speed and low-power superconducting neuromorphic circuits based on quantum phase-slip junctions," *IEEE Trans. Appl. Supercond.*, 2021, doi: 10.1109/TASC.2021.3066194.
- [74] E. Toomey, K. Segall, M. Castellani, M. Colangelo, N. Lynch, and K. K. Berggren, "Superconducting Nanowire Spiking Element for Neural Networks," *Nano Lett.*, vol. 20, no. 11, pp. 8059–8066, 2020, doi: 10.1021/acs.nanolett.0c03057.
- [75] E. Toomey, K. Segall, and K. K. Berggren, "A power efficient artificial neuron using superconducting nanowires," *arXiv*, 2019.
- [76] R. Cheng, U. S. Goteti, and M. C. Hamilton, "Superconducting neuromorphic computing using quantum phase-slip junctions," *IEEE Trans. Appl. Supercond.*, vol. 29, no. 5, pp. 1–5, 2019, doi: 10.1109/TASC.2019.2892111.
- [77] E. Toomey, Q. Y. Zhao, A. N. McCaughan, and K. K. Berggren, "Frequency Pulling and Mixing of Relaxation Oscillations in Superconducting Nanowires," *Phys. Rev. Appl.*, 2018, doi: 10.1103/PhysRevApplied.9.064021.
- [78] J. M. Shainline, S. M. Buckley, R. P. Mirin, and S. W. Nam, "Superconducting Optoelectronic Circuits for Neuromorphic Computing," *Phys. Rev. Appl.*, vol. 7, no. 3, pp. 1–27, 2017, doi: 10.1103/PhysRevApplied.7.034013.
- [79] T. Yamamoto, "Quantum information processing with superconducting nanowire single-photon detectors," *IEICE Transactions on Electronics*, 2019, doi: 10.1587/transele.2018SDI0002.
- [80] H. Shibata, T. Hiraki, T. Tsuchizawa, K. Yamada, Y. Tokura, and S. Matsuo, "A waveguide-integrated superconducting nanowire single-photon detector with a spot-size converter on a Si photonics platform," *Supercond. Sci. Technol.*, 2019, doi: 10.1088/1361-6668/aaf84f.
- [81] S. Ferrari, C. Schuck, and W. Pernice, "Waveguide-integrated superconducting nanowire single-photon detectors," *Nanophotonics*, 2018, doi: 10.1515/nanoph-2018-0059.
- [82] S. Buckley *et al.*, "Design of Superconducting Optoelectronic Networks for Neuromorphic Computing," *2018 IEEE Int. Conf. Rebooting Comput. ICRC 2018*, vol. 1, pp. 1–7, 2019, doi: 10.1109/ICRC.2018.8638595.
- [83] S. M. Buckley *et al.*, "Optimization of photoluminescence from W centers in silicon-on-insulator," *arXiv*, pp. 2020–2021, 2019, doi: 10.1364/oe.386450.
- [84] J. M. Shainline *et al.*, "Superconducting optoelectronic loop neurons," *J. Appl. Phys.*, vol. 126, no. 4, 2019, doi: 10.1063/1.5096403.
- [85] J. M. Shainline *et al.*, "Superconducting optoelectronic neurons III: Synaptic plasticity," *arXiv*, vol. 80305, no. c, pp. 1–17, 2018.
- [86] I. I. Soloviev *et al.*, "Adiabatic superconducting artificial neural network: Basic cells," *J. Appl. Phys.*, vol. 124, no. 15, 2018, doi: 10.1063/1.5042147.
- [87] S. Kumar, J. P. Strachan, and R. S. Williams, "Chaotic dynamics in nanoscale NbO₂ Mott memristors for analogue computing," *Nature*, 2017, doi: 10.1038/nature23307.
- [88] Y. S. Kim, Y. Cho, P. M. Nogales, and S. K. Jeong, "NbO₂ as a noble zero-strain material for li-ion batteries: Electrochemical redox behavior in a nonaqueous solution," *Energies*, 2019, doi: 10.3390/en12152960.
- [89] R. L. Fagaly, "Superconducting quantum interference device instruments and applications," 2006, doi: 10.1063/1.2354545.
- [90] P. Y. Chen, J. S. Seo, Y. Cao, and S. Yu, "Compact oscillation neuron exploiting metal-insulator-transition for neuromorphic computing," 2016, doi: 10.1145/2966986.2967015.
- [91] M. Davies *et al.*, "Loihi: A Neuromorphic Manycore Processor with On-Chip Learning," *IEEE Micro*, 2018, doi: 10.1109/MM.2018.112130359.
- [92] M. V. Debole *et al.*, "TrueNorth: Accelerating From Zero to 64 Million Neurons in 10 Years," *Computer (Long. Beach. Calif.)*, 2019, doi: 10.1109/MC.2019.2903009.
- [93] D. S. Holmes, A. L. Ripple, and M. A. Manheimer, "Energy-Efficient Superconducting Computing—Power Budgets and Requirements," *IEEE Trans. Appl. Supercond.*, vol. 23, no. 3, pp. 1701610–1701610, Feb. 2013, doi: 10.1109/TASC.2013.2244634.
- [94] O. A. Mukhanov, D. Gupta, A. M. Kadin, and V. K. Semenov, "Superconductor analog-to-digital converters," 2004, doi: 10.1109/JPROC.2004.833660.
- [95] M. Radparvar *et al.*, "Superconductor analog-to-digital converter for high-resolution magnetic resonance imaging," *IEEE Trans. Appl. Supercond.*, 2015, doi: 10.1109/TASC.2014.2361132.
- [96] D. Gupta, A. A. Inamdar, D. E. Kirichenko, A. M. Kadin, and O. A. Mukhanov, "Superconductor analog-to-digital converters and their applications," 2011, doi: 10.1109/MWSYM.2011.5972910.
- [97] M.-W. Kwon, M.-H. Baek, S. Hwang, S. Kim, and B.-G. Park, "Spiking Neural Networks with Unsupervised Learning Based on STDP Using Resistive Synaptic Devices and Analog CMOS Neuron Circuit," *J. Nanosci. Nanotechnol.*, 2018, doi: 10.1166/jnn.2018.15700.
- [98] C. L. Ayala, T. Tanaka, R. Saito, M. Nozoe, N. Takeuchi, and N. Yoshikawa, "MANA: A Monolithic Adiabatic iNtegration Architecture Microprocessor Using 1.4-zJ/op Unshunted Superconductor Josephson Junction Devices," *IEEE J. Solid-State Circuits*, 2021, doi: 10.1109/JSSC.2020.3041338.
- [99] S. Alam, M. S. Hossain, and A. Aziz, "A non-volatile cryogenic random-access memory based on the quantum anomalous Hall effect," *Sci. Rep.*, 2021, doi: 10.1038/s41598-021-87056-7.
- [100] S. Peotta and M. Di Ventra, "Superconducting Memristors," *Phys. Rev. Appl.*, 2014, doi: 10.1103/PhysRevApplied.2.034011.
- [101] S. Alam, M. S. Hossain, and A. Aziz, "A cryogenic memory array based on superconducting memristors," *Appl. Phys. Lett.*, vol. 119, no. 8, p. 082602, Aug. 2021, doi: 10.1063/5.0060716.